# Multipath Propagation Analysis for Vehicle-to-Infrastructure Communication at 60 GHz

Ales Prokes\*, Jiri Blumenstein\*, Josef Vychodil\*, Tomas Mikulasek\*, Roman Marsalek\*, Erich Zöchmann†‡\*, Herbert Groll‡, Christoph F. Mecklenbräuker‡, Thomas Zemenx, Aniruddha Chandra‡, Hussein Hammoud††, Andreas F. Molisch††

\*Department of Radio Electronics, Brno University of Technology, Czech Republic, prokes@vutbr.cz

† Christian Doppler Laboratory for Dependable Wireless Connectivity for the Society in Motion

‡ Institute of Telecommunications, TU Wien, Austria

\* Safety and Security Department, Austrian Institute of Technology, Austria

†National Institute of Technology, Department of Electronics and Communication Engineering, India

†† Wireless Devices and Systems Group, University of Southern California, USA

Abstract— The paper deals with an analysis of multipath propagation environment in the 60 GHz band using a pseudorandom binary sequence-based time-domain channel sounder with 8 GHz bandwidth. The main goal of this work is to analyze the multipath components (MPCs) propagation between a moving car carrying a transmitter with an omnidirectional antenna and a fixed receiver situated in a building equipped with a manually steered directional horn antenna. The paper briefly presents the time dependence of the dominant MPC magnitudes, shows the effect of the surrounding vegetation on the RMS delay spread and signal attenuation, and statistically evaluates the reflective properties of the road which creates the dominant reflected component. To understand how the MPCs propagate through the channel we measured and analyzed the power and the RMS delay spread distributions in the static environment surrounding the car using an automated measuring system with a controlled receiver antenna tracking system. We give some examples of how the MPC magnitudes change during the antenna tracking and demonstrate that a building and a few cars parked close to the measuring car create a lot of MPCs detectable by the setup with a dynamic range of about 50 dB.

Keywords—millimeter wave, channel measurement, channel sounder, channel impulse response, delay spread.

# I. INTRODUCTION

Automated driving systems of future vehicles will be much more reliable and safer when employing inter-vehicular communication [1]. Being able to disseminate information on safety-critical events detected or caused by individual participants in the traffic with other relevant traffic members is for sure beneficial not only in terms of safety, but also in terms of traffic flow and overall smoothness of the transportation process. The vehicle-to-vehicle communication (V2V) had been previously studied for various sub-6 GHz frequency bands [2]; however, it is tempting to utilize specific parts of a much higher frequency band designated as the millimeter wave (MMW) band, which spans the frequency range 30-300 GHz. Many studies consider especially the frequency band around 60 GHz

because the International Telecommunication Union (ITU) assigns the 60 GHz band to the Industrial, scientific and medical (ISM) bands allowing license-free operations and offers several GHz of bandwidth, which is unheard of in the mentioned sub-6 GHz band [3].

It needs to be mentioned that the 60 GHz band for vehicular connectivity had been studied several decades earlier, see e.g. [4], however, in a very narrowband setup leading to the fact that the extensive bandwidth, available in the already mentioned 60 GHz band, stayed unused. At present, as the advances in the monolithic microwave integrated circuitry (MMIC) have brought the attention of both the industrial and the scientific community again to the 60 GHz band, the V2V MMW communication is revisited, for example in [5]. The path-loss of the links at 60 GHz is of course still high due to the oxygen absorption in the atmosphere which reaches 15 dB/km; therefore it is deemed suitable for short-range communication rather than for long-range backhauls [6]. The broadband V2V MMW communication is studied in [7] demonstrating exemplary power-delay profiles (PDPs), path-loss and root-mean-square (RMS) delay spreads of the radio channel between two oncoming vehicles. In [7], the information exchange is direct. without any intermediary. In this paper, we show another possible scenario termed vehicle-to-infrastructure (V2I), where the information from the individual vehicles is gathered by the (usually elevated) roadside infrastructure. Subsequently, the information might be backhauled to a distant area (e.g. in difficult non-line-of-sight situations (NLOS)) or transmitted back to other vehicles even in the vicinity of the original transmitter car. This relaying scenario might be beneficial due to the elevated installation of the roadside infrastructure, thus easing the issues of shadowing by other vehicles on the road [8].

In [9], the V2I scenario, where the transmitter and the receiver are not moving but the surrounding traffic on the two-lane road causes the time-varying nature of the channel, is analyzed. It is shown in [9] that the presence of moving vehicles,

although making the channel non-stationary, may reduce the RMS delay spread. This is due to the presence of cars, which effectively serve as artificial reflecting surfaces and thus increase the total received power.

In [10], the outage probability of MMW V2I propagation channels is researched with the conclusion that the two-wave Rice model is not necessary and "the road-reflected wave can be neglected in the numerical computations". The conclusions in [10] are based on a ray-tracing analytical channel model. On the other hand, however, based on the real-world channel sounding campaign in [5], a two-way diffuse power (TWDP) channel model is derived and validated via Akaike's information criterion. In [11], a small-scale fading model is derived for a V2I scenario similar to that in [5] and again, the TWDP statistics are confirmed. The two-way nature of the V2I MMW channel is also observed in this paper; however, here we show different statistical properties of the reflected path as compared with the line of sight (LOS).

With this background, the detailed contributions of this paper are as follows:

- Analysis of multipath components (MPCs) propagating between a moving car and a receiver situated in a building in terms of time dependence of direct and reflected MPCs magnitudes, RMS delay spread of the received MMW signal, and statistical evaluation of the strongest reflected component.
- Examination of 2D power and the RMS delay spread distributions in a static environment surrounding the car.

The rest of the paper is organized as follows. Section 2 briefly describes the channel sounder. Section 3 informs about the measurement scenarios used for time-varying and static environments. Section 4 deals with the real word measurements. Then in Section 5, the analyses of both the time-varying and the static channels are presented. A summary of the paper is given in the conclusion.

#### II. MEASUREMENT SETUP

The channel measurement was carried out using the 60 GHz time-domain channel sounder described in detail in [12]. It is composed of a pseudo-random binary sequence (PRBS) transmitter (TX) and a correlation receiver (RX). It employs Golay complementary sequences as the excitation PRBS signal, because of their very good correlation properties, minimal leakage effects caused by FFT [13], and a great ability to mitigate unwanted nonlinearity effects produced by channel sounder analog circuits [14]. The transmitter is based on an Anritsu MP1800A Signal Quality Analyzer working as a PRBS generator. The receiver is created using a Tektronix MSO72004C (20 GHz, 50 GS/s) Mixed Signal Oscilloscope working as a very fast analog-to-digital converter. The baseband PRBS signal is converted into the MMW band and back using SiversIma FC1000V series V-band up/down converters [15]. The channel sounder bandwidth is 8 GHz, the number of samples per measured channel impulse response (CIR) is set to  $N_{Sa} = 8092$  and the number of saved CIRs per measurement is

 $N_{CIR} = 932$ . Due to the correlation gain the sounder dynamic range is about 45 dB. In the case of static channel measurement, it can be increased by another 5-10 dB using an averaging technique. Downloading data from the oscilloscope to a PC, and their basic processing are controlled by LabView.

The transmitter was equipped with an omnidirectional SIW slot antenna described in [16], whose radiation pattern related to the car is shown in Fig. 1. An angle of 0° in both the E- and the H-plane corresponds to the left side of the car (as seen by the driver) and the car roof in the H-plane is situated at an angle of 270°. The MMW signal was received using a directional horn antenna with a dielectric lens. The antenna gain dependence on the angle is shown in Fig. 2.

All measured values mentioned below are related to the low noise MMW preamplifier output. The following down converter SiversIma then increases them by a gain of about 15-20 dB.

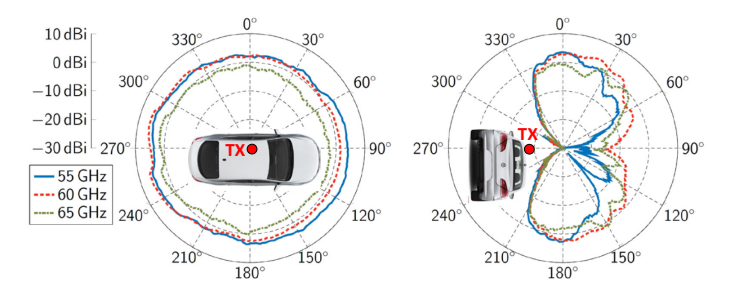


Fig. 1. E-plane (left) and H-plane (right) measured radiation pattern of double-sided SIW slot antenna at 55 GHz, 60 GHz, and 65 GHz.

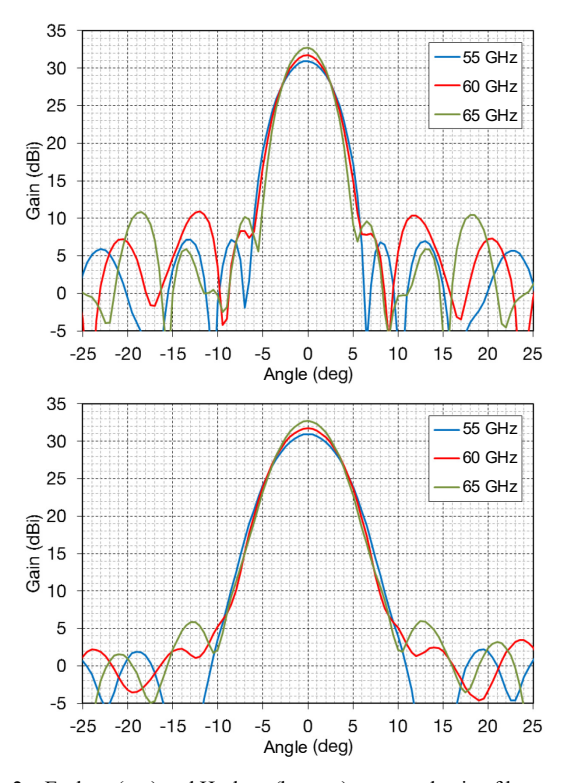


Fig. 2. E-plane (top) and H-plane (bottom) measured gain of horn antenna with dielectric lens at 55 GHz, 60 GHz, and 65 GHz.

## III. MEASUREMENT SCENARIOS

All V2I measurements were performed in the Brno University of Technology campus between the building at Technicka 12 and a VW CC car driving on the road in front of the building as shown in Fig. 3. The car was moving in both directions at different speeds. In the text below, we will use the designation "Scenario 1a" for the direction of moving shown in Fig. 3 and "Scenario 1b" for the opposite direction of the car movement. Since the measured results contained several multipath components whose origin was ambiguous, we made further stationary measurements in order to be able to correctly interpret the measured data. In "Scenario 2" the car was situated in front of the building and the channel was scanned by the horn antenna directed to uniformly distributed points as shown in Fig. 4. To determine the direction of propagation of certain MPCs, the TX antenna was in a few measurements shielded towards the receiver by an MMW absorber as shown in the upper left corner.

In all the scenarios the transmitter was situated in the car and its antenna together with the power amplifier and cooler were placed on the car roof as shown in Fig. 5 (left). The receiver was situated in a room on the 6th floor of the university building. In Scenarios 1a and 1b the RX antenna was mounted on a photographic gimbal head and tripod and directed out of an open window (see Fig. 5 (middle)). The antenna was manually directed to the moving car using a riflescope. This manual tracking of the directional antenna simulates electronic beam steering of an antenna array assumed for 5G wireless networks [17]. The correctness of the horn antenna alignment was checked using a video recorded by a camera mechanically coupled to the antenna. In Scenario 2 the RX antenna was directed using a motorized Sky-Watcher AllView mount (see Fig. 5 (right)) controlled by PC and LabView.

For Scenarios 1a and 1b the car speed was chosen v = 30 km/h to 50 km/h. As shown in Fig. 3, the height of the TX and RX antennas above the ground is h = 1.55 m and H = 14.5 m respectively. It is obvious that for Scenario 1a, where the distance between the TX antenna and the building is D = 28.5 m, the propagation distance between the antennas is  $L = \sqrt{(H - h)^2 + D^2} = 31.3$  m. Similarly, for Scenario 1b, where D is only 25 m because the car goes on the roadside closer to the building, we can get L = 28 m.

# IV. MEASUREMENT

For all the car speeds and directions, we had performed three measurements and then we selected the measurement where the car tracking was the most accurate. Note that the tracking of a moving car is not easy especially at higher speeds. The magnification of the telescope must not be too high, as it must allow the car to be quickly found. In such a case, the transmitter is too small for watching. Thus, in most cases the RX antenna was directed to the car center (to the bottom part of the doors). Examples of measured CIRs for Scenario 1a, are shown in Fig. 6, where for a clearer interpretation of the results we used the propagation distance at the vertical axis instead of the more common time or delay.

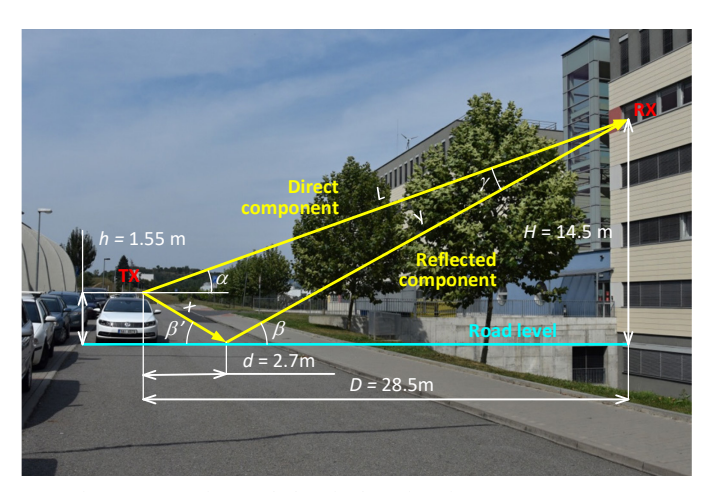


Fig. 3. Measuring workplace in the university campus at Technická 12, Brno

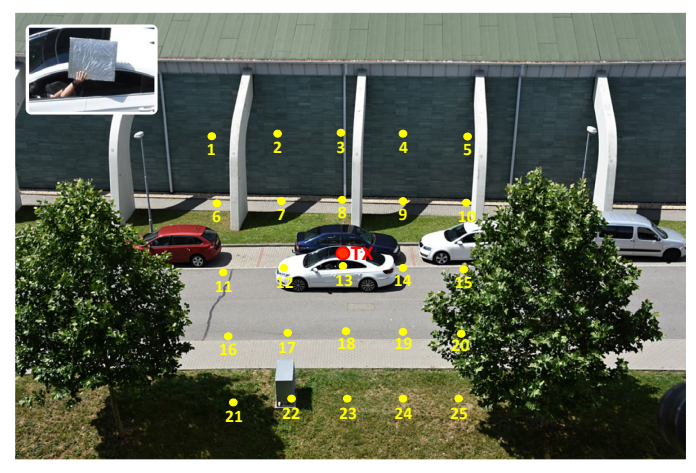


Fig. 4. Distribution of the measurement points for CIR evaluation.

First, we chose a long period of CIRs measurement  $T_{CM} = 5$  ms and the car speed v = 50 km/h to be able to observe changes in the MPCs and the influence of surrounding trees on signal propagation. The corresponding total measurement time  $T_{TM} = T_{CM} \times N_{CIR}$  was 4.675 s. Further, to analyze the influence of the road roughness on the MMW signal reflection during the car movement we set the measurement period to  $T_{CM} = 200 \, \mu \text{s}$  which gives the total measurement time  $T_{TM} = 0.186 \, \text{s}$ . For  $v = 50 \, \text{km/h}$  ( $v = 14 \, \text{m/s}$ ) the CIRs are taken every  $v \times T_{CM} = 2.8 \, \text{millimeters}$  of the car movement.



Fig. 5. From left to right: placement of TX antenna on the car roof, RX antenna on the gimbal head and on the motorized mount.

It is obvious that in both cases there are two dominant components: a direct component (the stronger and nearer one) and a reflected component. To find a reflective spot, we parked the car at the position shown in Fig. 4 and placed the MMW absorber on the road, sidewalk and various parts of the car. We observed that this component was reflected off the road at about 2.7 meters from the car as shown in Fig. 3. The difference between the direct and reflected path lengths  $\Delta L = x + y - L =$  $\sqrt{d^2 + h^2} + \sqrt{(D-d)^2 + H^2} - L$  is then 1.4 m, which corresponds to the measured difference shown in Fig. 6. The angle between the direct component and the reflected component is  $\gamma = 4.95^{\circ}$ . It is given by  $\gamma = \beta - \alpha =$ arctg[H/(D-d)] - arctg[(H-h)/D]. Note that the angles  $\beta$ and  $\beta'$  slightly differ because the road is not perfectly even. As the maximum measurable distance of the channel sounder is 49 m [12], the multipath components propagating over a longer distance (multiply reflected from the building behind the car) are aliased as shown in Fig. 6. The white dashed curves approximate the maximum MPCs position (see below). The measurements were made so that the center of records corresponded to the moment when the transmitter and the receiver were both in a vertical plane perpendicular to the building wall. Different distances at the beginning and the end of record shown in Fig. 6 (top) are caused by an imperfect parallelism of the road and the building.

In Scenario 1b, when the car was moving in the opposite direction, the data records are very similar to those shown in Fig. 6 (top), but there is no component reflected from the road since the road and the sidewalk were shadowed by the car roof.

Scenario 2 measurements were performed for several car positions. The most interesting measurement (the richest in MPC components) is shown in Fig. 4. To get information about the MPCs power distribution in 2D plane we used the motorized mount and scanned the space around the transmitter in rectangular coordinates with horizontal and vertical steps of 5°. Since the measurement setup was working in the same way as in Scenario 1 but it recorded only 100 CIRs for any measurement point, we averaged them to increase the signal to noise ratio (SNR). We evaluated the power at all points by summing the CIR peaks above the noise floor, which was set to -60 dBV. A smooth representation of the distribution, shown in Fig. 7, was achieved by interpolating the values by a ratio of 32. The elongated shape in the vertical direction is caused by strong MPCs reflected by the car and the building behind the transmitter and by the road. Of non-negligible influence are also the different beam-widths of the RX antenna in the vertical and the horizontal axes as shown in Fig. 2.

# V. CHANNEL CHARACTERIZATION

As mentioned above the aim of this work is to analyze the time varying MPC characteristics caused by a moving car such as MPC magnitude variation in time, its statistical properties, and the time variation of the delay spread. Another research goal is to analyze the power and RMS delay spread distributions in a static environment surrounding the car and to find any dependence between them. So, we can divide the channel characterization into two subsections devoted to the time-varying and the static channels.

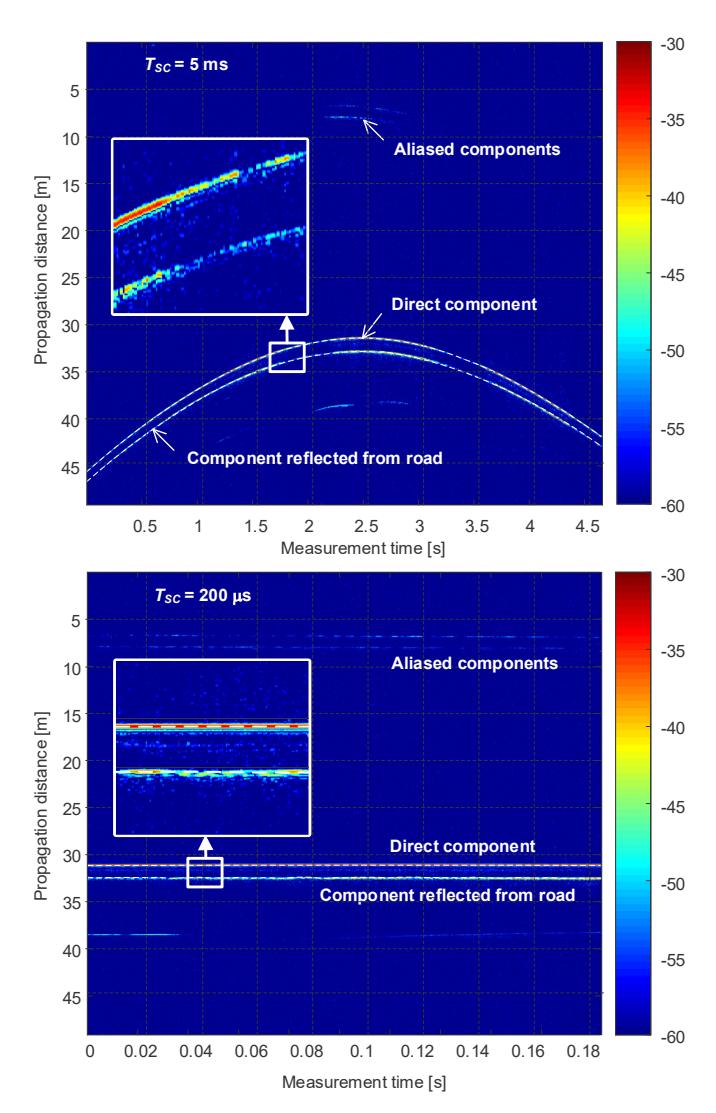


Fig. 6. The CIR magnitude in dBV measured in Scenario 1a with sampling periods  $T_{SC}$ = 5 ms (top) and and  $T_{CM}$ = 200 µs (bottom).

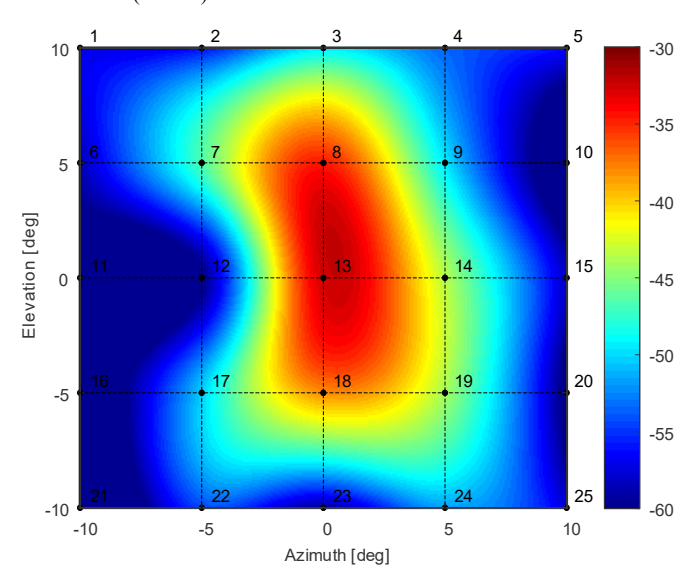


Fig. 7. Power distribution in the vinicity of the car.

#### A. Analysis of time-varying channel

To analyze the MPCs magnitude variation we approximated the coordinates (indices) of direct and reflected components by a smooth curve as shown in Fig. 6. It was accomplished by the following three steps:

- Detecting the strongest and the second strongest component (i.e. the direct component and the component reflected from the road) in each CIR record and determining their coordinates.
- Filtering the coordinates by a Hampel filter to remove outliers (coordinates of the other higher components not belonging to the two above).
- Filtering the coordinates using a Savitzky-Golay FIR filter to obtain a smooth approximation.

The Hampel filter is a configurable-width sliding window filter, calculating for each window the median and the standard deviation  $\sigma$ . If any point in the window is more than  $n\sigma$  out of the median, where n is a user-definable value (default n=3), then the Hampel filter identifies this point as an outlier and replaces it with the median. Compared with a simpler median filter the Hampel filter is defined by another parameter  $(n\sigma)$ , which improves the filter configurability and offers better fitting. Both the window length and n were set empirically.

The Savitzky-Golay filter is a frequently used smoothing filter based on local least-squares polynomial approximation. The filter is defined by the polynomial order and by the approximation interval. Optional parameters implemented in MATLAB, which was used for simulations, are positive-valued weights used during the least-squares minimization. Thanks to many configurable parameters, it can be very well optimized for the desired approximation. The filter is necessary to approximate the signal tendency when its magnitude is strongly attenuated (for example when the signal penetrates trees) and when the Hampel filter does not give a satisfactory result. In fact, both filters represent the momentum of the car and smooth the curves representing the distance change.

The time dependence of the direct and reflected component magnitudes depicted in Fig. 6 (top) plotted for the fitted coordinates is shown in Fig. 8 (grey waveforms). The time dependence of the direct component obtained in Scenario 1b is then shown in Fig. 9. The trends (black and red dashed waveforms) were obtained by lowpass zero-phase bidirectional filtering, where the data is processed in both the forward and the reverse directions, which does not shift the filtered signal in time.

The effect of trees in Figs 8 and 9 is obvious. The attenuation varies in a wide range, depending on which part of treetops the MMW signal penetrates. Its maximum is slightly above 30 dB. Note that the difference in the magnitudes between the direct and the reflected component in Scenario 1a is relatively small. In the "unshadowed" record segments the trends differ between 6-12 dB. As mentioned above it is caused by pointing the traced RX antenna at the car doors.

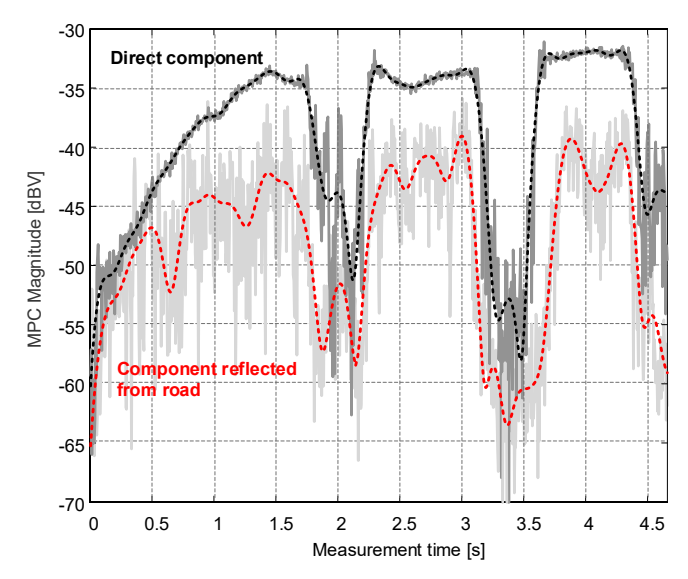


Fig. 8. The time dependence of the direct and reflected component magnitudes measured in Scenario 1a for  $T_{VM} = 5$  ms.

The ripple of the direct component magnitude is due to imperfect manual tracking and angularly dependent TX antenna irradiation (see Fig. 1). The ripple of the reflected component magnitude is additionally affected by road irregularities. Note that the bottom parts of component magnitudes are also affected by the measurement setup noise.

The effect of the road on a reflected component is also obvious in Fig. 10, where the component magnitudes depicted in Fig. 6 (bottom) are plotted. While the small changes in the direct component magnitude are caused by the receiver noise, downconverter IQ imbalance, and possibly by the phase noise of the reference rubidium oscillators, the larger variation of the reflected component is caused predominantly by the rough road surface (flat asphalt). To confirm this, one measurement was performed with the stationary vehicle and compared with all the time-varying channel measurements (made at different speeds between 40 and 50 km/h) with respect to the reflected component magnitude variance. The reflected component for the stationary car is shown in Fig. 10 (blue waveform). It can be concluded that the influence of receiver noise is small as the variance (normalized power in W) of the reflected component measured for a stationary car is 2.08e-07 while the variance of the reflected component measured for a moving car is in the interval from 2.30e-05 to 7.85e-06. Note that the direct component variance in the static measurement is 2.10e-07.

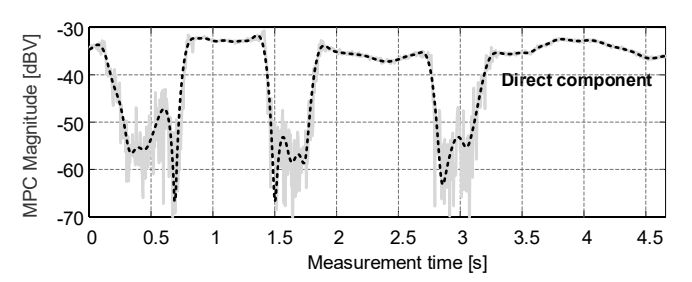


Fig. 9. The time dependence of the direct component magnitudes measured in Scenario 1b for  $T_{CM}$ = 5 ms.

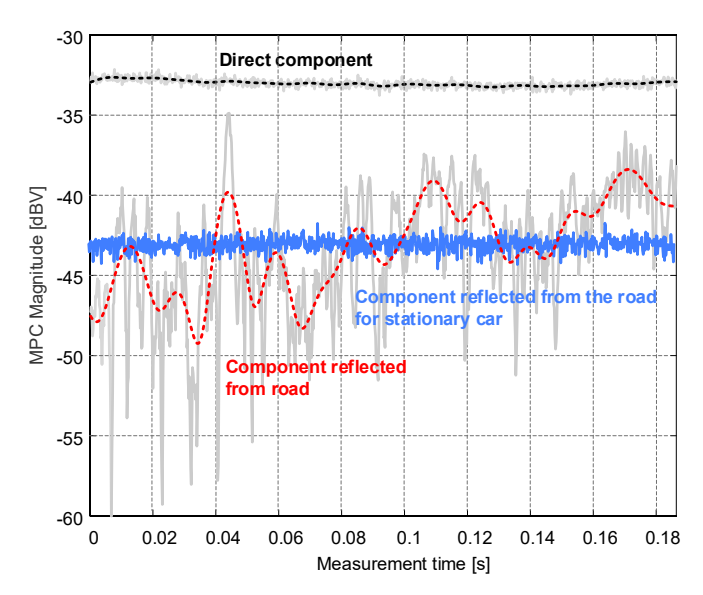


Fig. 10. The time dependence of the LOS and reflected component magnitudes measured in Scenario 1a for  $T_{CM}$ = 200  $\mu$ s.

Another aim of the channel characterization was to fit the distribution of the reflected component magnitudes by a proper probability density function (PDF). It was found that the best fitting can be obtained by a generalized extreme value (GEV) distribution given by the location parameter  $\mu$ , scale parameter  $\sigma$ , and shape parameter  $k \neq 0$ . For all four unfiltered datasets we defined intervals for the above parameters:  $\mu \in \langle 4.4 \text{ mV},$ 5.8 mV),  $\sigma \in \langle 2.3 \text{ mV}, 4.0 \text{ mV} \rangle$ , and  $k \in \langle -0.055, -0.108 \rangle$ . No relationship between the amplitude distribution and the speed of the vehicle was found. The PDF calculated as a histogram, and the cumulative distribution function (CDF) of the reflected component depicted in Fig. 10 (gray waveform), fitted by the GEV distribution are shown in Fig. 11. Note that when the filtered trend (red curve) is subtracted from an unfiltered record (gray waveform) the result can be successfully fitted with the normal distribution. In other words, the effect of small particles in asphalt can be fitted by a normal distribution.

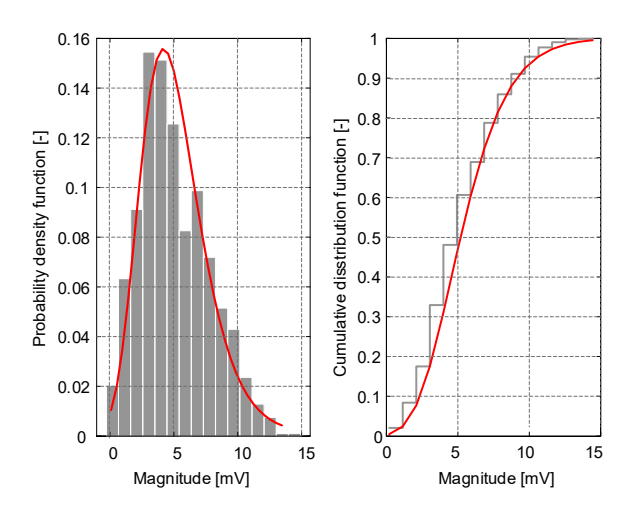


Fig. 11. PDF (left) and CDF (right) calculated and fitted by generalized extreme value distribution for the component reflected from the road.

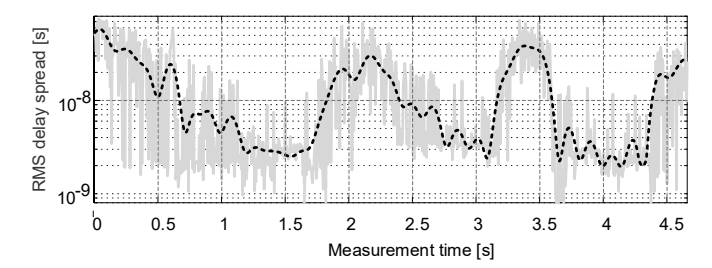


Fig. 12. The time dependence of the instantaneous RMS delay spread for  $T_{CM}=5$  ms.

Finally, we calculated the instantaneous RMS delay spread for the components depicted in Fig. 6 (top) according to [18]

$$\sigma_{\tau,t} = \left[ \frac{\sum_{i=1}^{L} |h(\tau_{i},t)|^{2} \tau_{i}^{2}}{\sum_{i=1}^{L} |h(\tau_{i},t)|^{2}} - \frac{\left(\sum_{i=1}^{L} |h(\tau_{i},t)|^{2} \tau_{i}\right)^{2}}{\left(\sum_{i=1}^{L} |h(\tau_{i},t)|^{2}\right)^{2}} \right]^{\frac{1}{2}}, \quad (1)$$

where  $|h(\tau_i, t)|$  are the magnitudes of CIR taps at the delay  $\tau_i$ , t is the measurement time (capturing time of CIRs), and L is the number of taps. The number of taps was chosen experimentally as the number of the CIR peaks exceeding the receiver noise threshold (-60 dBV). The RMS delay spread plotted in the logarithmic vertical scale is shown in Fig. 12. It corresponds well to the magnitudes in Fig. 8. The range of averaged values (black dashed waveform) between 2 ns (LOS propagation) and 60 ns (shadowing by trees) are typical of outdoor V2X scenarios [19]. By applying FFT to the complex values of the component reflected from the road we found that at speeds of up to 50 km/h, the significant components do not exceed the 600 Hz as evident from Fig. 13.

# B. Analysis of static channel

The aim of the static channel analysis is to find how some MPCs propagate through the channel in order to correctly interpret the data measured and to find some dependence between the received signal power and the RMS delay spread. For this purpose, we first calculated the power distribution in the car vicinity as mentioned above and shown in Fig. 7, and then evaluated the RMS delay spread for all the measured points according to (1). A map of the RMS delay spread distribution is shown in Fig. 14. It is evident that the minimum value occurs very close to the transmitter (point 13), due to the dominant direct component. The relatively low delay spread at points 8, 12, 14 and 18 is caused by the presence of direct components and either strong MPCs traveling close to the direct component (reflected from the road) or weak MPCs traveling far from the direct component (e.g. reflected from the building behind the transmitter).

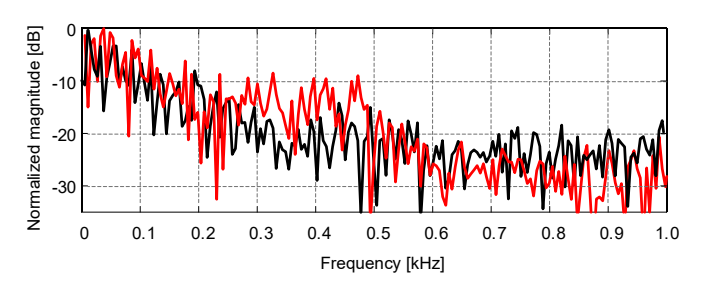


Fig. 13. Spectrum of reflected component measured in Scenario 1a for  $T_{SC}$ = 200  $\mu$ s and the car speed  $\nu$  = 40 km/h (black) and  $\nu$  = 50 km/h (red).

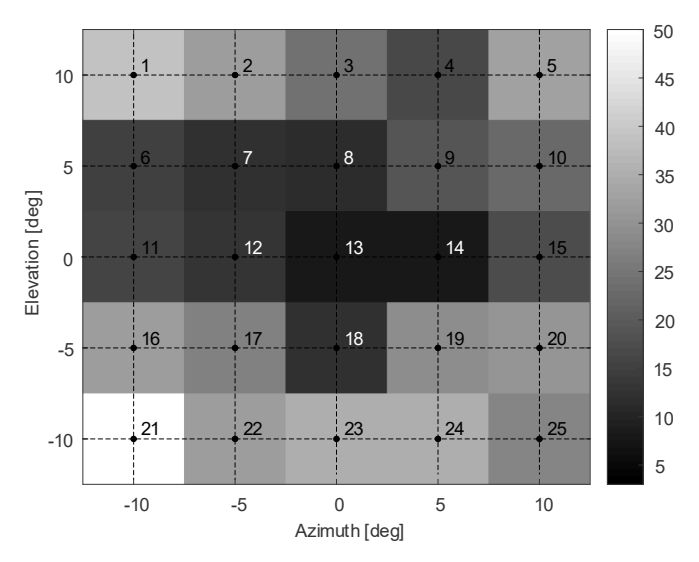


Fig. 14. Map of RMS delay spread in nanoseconds calculated for a set of CIRs measured in the vinicity of the car.

The CIRs corresponding to points 13 and 18 are shown in Fig. 15. The black waveforms were measured without the MMW absorber and the red waveforms were obtained with the absorber shielding the TX antenna. The blue circles indicate the values used for the calculation. It is obvious that the component C was reflected from the building behind the transmitter, because it was also received with the absorber, while the component D propagated towards the receiver and it was probably multiply reflected. The difference between the points 13 and 18 is 5° in the vertical direction. This difference causes a noticeable changes in the direct component A (13 dB) and in the component reflected from the road (7 dB). This unequal difference in the changes is due to the angle depended RX antenna gain and the deviation of the position of central point 13 and the transmitter as shown in Fig. 4.

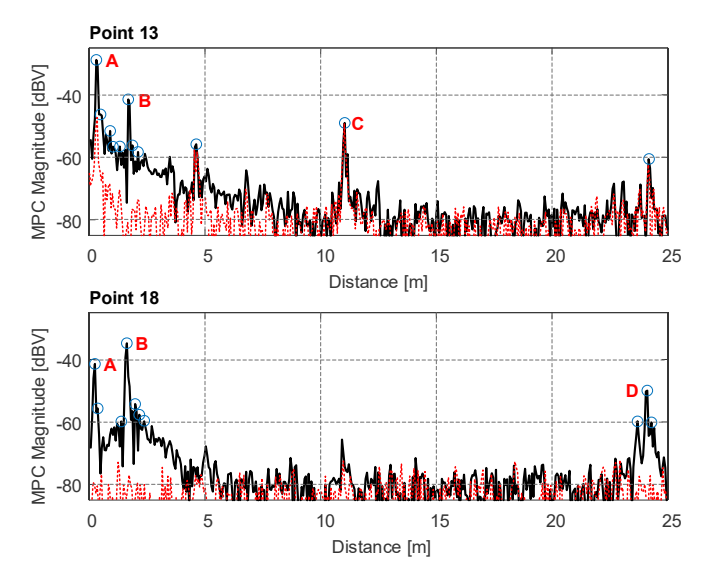


Fig. 15. The CIRs obtained at points 13 and 18 without (black) and with (red) absorber.

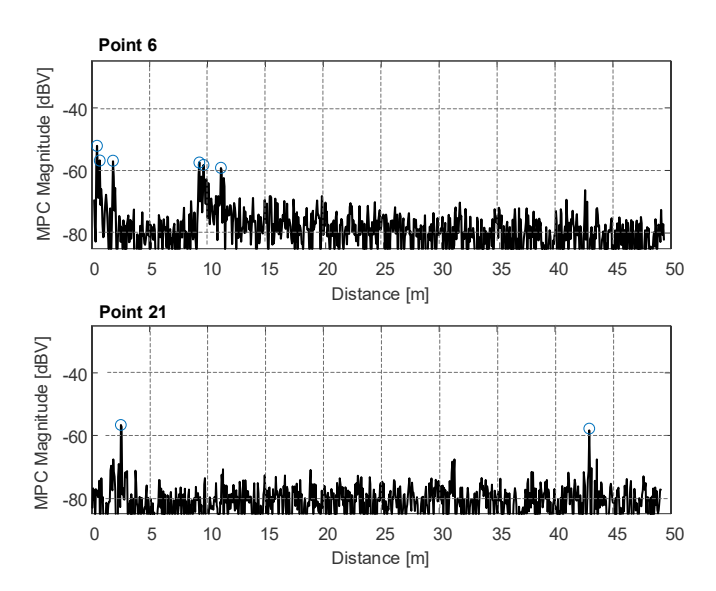


Fig. 16. The CIRs obtained at the edge points 6 and 21.

The averaging effect implemented in this measurement increases the dynamic range and allows detecting many weak MPCs. Thanks to it we can evaluate the RMS delay spread also for the edge points (far from the transmitter). An example of the CIRs measured for the edge points with the highest and the lowest RMS delay spread is shown in Fig. 16. The highest RMS delay spread at point 21 is caused by a two very distant peaks with similar power.

Comparing the power distribution depicted in Fig. 7 and the RMS delay spread shown in Fig. 14 we can conclude that there is no easily describable dependence between power and delay spread of received signal except point 13. Note that in the case of the RX antenna with a broader beam-width the RMS delay spread would be probably higher.

# VI. CONCLUSION

We analyzed the multipath components propagation between a moving car on a road and a fixed receiver situated in a campus building. We showed very good reflective properties of the asphalt surface and demonstrated them by the small difference between the direct and the reflected component magnitudes varying between 6-17 dB (see Fig. 8 and Fig. 10). Similar small difference lower than 12 dB can also be observed between these components in "static scenario" (Fig. 15). Then we examined the attenuation caused by trees. We discovered that it varies in a wide range and its maximum for all the measurements slightly exceeds the value 30 dB. The time variation of the reflected component magnitudes was fitted by a generalized extreme value distribution and the marginal values of the distribution parameters were found for all the measurements. For "moving scenario" we then evaluated the time dependence of the RMS delay spread. We found that its averaged values (trends) vary in the range from 2 ns (obtained for obstructed LOS propagation) to 60 ns (obtained for the case the signal shadowed by trees). Finally, we calculated the spectrum of the component reflected from the road and discovered that at speeds of up to 50 km/h, there are no significant components above 600 Hz.

To understand how the MPCs propagate through the channel we measured and analyzed the power and the RMS delay spread distributions in the static environment surrounding the car. We obtained very similar values of the RMS delay spread between 3 and 50 ns as in the case of the previous time-varying channel analysis. We justified these values by analyzing the multipath component in the corresponding CIRs. Finally, by analyzing the 2D power and the RMS delay spread distribution we came to the conclusion that there is no provable relationship between them. By the results presented we generally demonstrate that a building and a few cars parked close to the measuring car create an environment relatively rich in multipath components.

#### ACKNOWLEDGMENT

The research described in this paper was financed by the Czech Science Foundation, Project No. 17-27068S, by the National Sustainability Program under grant LO1401 and by the California Transportation Authority under the METRANS program. For the research, the infrastructure of the SIX Center was used.

#### REFERENCES

- C. Sommer and F. Dressler, Vehicular networking, Cambridge University Press, 2015.
- [2] C. F. Mecklenbrauker et al., "Vehicular Channel Characterization and Its Implications for Wireless System Design and Performance," *Proceedings* of the IEEE, July 2011.
- [3] ITU, "Radio Regulations, Section IV. Radio Stations and Systems Article 1.15, definition: Industrial, scientific and medical (ISM) applications (of radio frequency energy)".
- [4] H. Meinel and A. Plattner, "Millimetre-wave propagation along railway lines," *IEE Proceedings F (Communications, Radar and Signal Processing)*, no. 130, p. 688–694, 1983.
- [5] E. Zöchmann et al., "Position-Specific Statistics of 60 GHz Vehicular Channels During Overtaking," *IEEE Access*, vol. 7, pp. 14216–14232, 2019.
- [6] M. Khatun, H. Mehrpouyan and D. Matolak, "60-GHz Millimeter-Wave Pathloss Measurements in Boise Airport," in *IEEE Global Conference* on Signal and Information Processing (GlobalSIP), pp. 1276–1280, 2018.

- [7] J. Blumenstein, et al., "Vehicle-to-Vehicle Millimeter-Wave Channel Measurements at 56-64 GHz," in *IEEE Vehicular Technology Fall Conference (VTC-Fall)* (accepted for publication), Honolulu, pp. 1–4, 2019.
- [8] M. G. Nilsson, D. Vlastaras, T. Abbas, B. Bergqvist and F. Tufvesson, "On multilink shadowing effects in measured V2V channels on highway," in 9th European Conference on Antennas and Propagation (EuCAP), Lisbon, 2015.
- [9] J. Blumenstein et al., "Measured High-Resolution Power-Delay Profiles of Nonstationary Vehicular Millimeter Wave Channels," in *IEEE 29th Annual International Symposium on Personal, Indoor and Mobile Radio Communications (PIMRC)*, Bologna, 2018.
- [10] R. Verdone, "Outage probability analysis for short-range communication systems at 60 GHz in ATT urban environments," *IEEE Transactions on Vehicular Technology*, vol. 46, no. 4, pp. 1027–1039, 1997.
- [11] E. Zöchmann, J. Blumenstein, R. Marsalek, M. Rupp, K. Guan: "Parsimonious Channel Models for Millimeter Wave Railway Communications", in *IEEE Wireless Communications and Networking Conference (WCNC)*, 2019, pp. 1 - 6.
- [12] A. Prokes et al., "Time-Domain Broadband 60 GHz Channel Sounder for Vehicle-to-Vehicle Channel Measurement," in 2018 IEEE Vehicular Networking Conference (VNC), Taipei, Taiwan, 2018, pp. 1–7.
- [13] R. Zetik, M. Kmec, J. Sachs, and R. S. Thomä, "Real-Time MIMO Channel Sounder for Emulation of Distributed Ultrawideband Systems," *Int. J. Antennas Propag.*, vol. 2014, Article ID 317683, pp. 1–16, 2014.
- [14] J. Vychodil, M. Pospisil, A. Prokes and J. Blumenstein, "Millimetre wave band time domain channel sounder," *IET Communications*, vol. 13, no. 3, pp. 331–338, 19 2 2019.
- [15] FC1005V/00 V-band Converter with LO. [Online]. Available: https://www.siversima.com/wp-content/uploads/FC1005V00-Data-Sheet.pdf. [Accessed: 15- Jun- 2018].
- [16] T. Mikulasek, J. Lacik, and Z. Raida, "SIW slot antennas utilized for 60-GHz channel characterization," *Microw Opt. Tech. Lett.*, vol. 57, no. 6, pp. 1365–1370, 2015.
- [17] S. Sun, T. S. Rappaport, R. W. Heath, A. Nix and S. Rangan, "Mimo for millimeter-wave wireless communications: beamforming, spatial multiplexing, or both?," *IEEE Communications Magazine*, vol. 52, no. 12, pp. 110–121, December 2014.
- [18] A. F. Molisch, "Statistical properties of the RMS delay-spread of mobile radio channels with independent Rayleigh-fading paths," in *IEEE Transactions on Vehicular Technology*, vol. 45, no. 1, pp. 201-204, Feb. 1996
- [19] E. Ben-Dor, T. S. Rappaport, Y. Qiao and S. J. Lauffenburger, "Millimeter-Wave 60 GHz Outdoor and Vehicle AOA Propagation Measurements Using a Broadband Channel Sounder," in *IEEE Global Telecommunications Conference* (GLOBECOM), Kathmandu, 2011, pp. 1–6.